# A Multi-Technique Reconfigurable Electrochemical Biosensor: Enabling Personal Health Monitoring in Mobile Devices

Alexander Sun, *Student Member, IEEE*, A. G. Venkatesh, and Drew A. Hall, *Member, IEEE*

***Abstract*—This paper describes the design and characterization of a reconfigurable, multi-technique electrochemical biosensor designed for direct integration into smartphone and wearable technologies to enable remote and accurate personal health monitoring. By repurposing components from one mode to the next, the biosensor's potentiostat is able reconfigure itself into three different measurements modes to perform amperometric, potentiometric, and impedance spectroscopic tests all with minimal redundant devices. A $3.9 \times 1.65$ cm$^2$ PCB prototype of the module was developed with discrete components and tested using Google's Project Ara modular smartphone. The amperometric mode has a $\pm$1 nA to $\pm$200 $\mu$A measurement range. When used to detect pH, the potentiometric mode achieves a resolution of $<$ 0.08 pH units. In impedance measurement mode, the device can measure 50 Ω–10 MΩ and has been shown to have $< 6^\circ$ of phase error. This prototype was used to perform several point-of-care health tracking assays suitable for use with mobile devices: 1) Blood glucose tests were conducted and shown to cover the diagnostic range for Diabetic patients (∼200 mg/dL). 2) Lactoferrin, a biomarker for urinary tract infections, was detected with a limit of detection of approximately 1 ng/mL. 3) pH tests of sweat were conducted to track dehydration during exercise. 4) EIS was used to determine the concentration of NeutrAvidin via a label-free assay.**

***Index Terms*—Electrochemical biosensor, glucose, Google Ara, lactoferrin, mHealth, pH, point-of-care, potentiostat, smartphone, sweat, wearables.**

## I. Introduction

CHRONIC illnesses, such as heart disease, stroke, cancer, and diabetes, are not only the leading cause of death and disability in the US, but also the most commonly diagnosed and expensive health issues to treat [1]. One of the many reasons for this phenomena is the heavy reliance on periodic hospital checkups as the sole mechanism to determine one's well-being. While remote and at-home testing is a promising solution to help alleviate this burden on the healthcare system and potentially improve one's health, most medical diagnostic equipment today is confined to centralized laboratories and hospitals. Furthermore, this equipment is too expensive and bulky for direct point-of-care (POC) use.

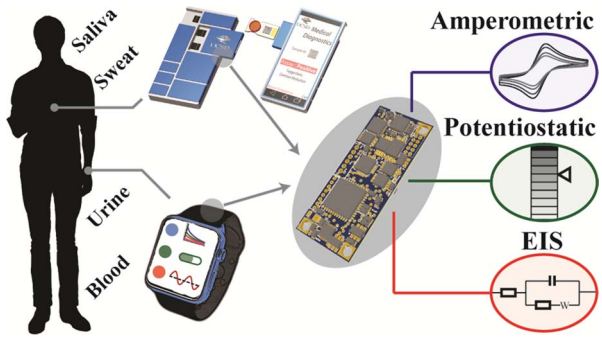


Fig. 1. Illustration showing potential uses for the multi-technique biosensor platform integrated into smartphones and wearable devices.

Fortunately, recent advances in portable electronics and sensor miniaturization have allowed for the development and proliferation of mobile health (mHealth) technologies that can continuously monitor patients at the POC, away from traditional hospital settings. Many mobile devices have fitness oriented sensors built-in, such as accelerometers for tracking physical activity, electrocardiograms (ECG) to record the electrical signals of the heart, and photoplethsymogram (PPG) to determine heart rate as well as the blood oxygenation level. Unfortunately, these sensors offer limited medically actionable data, especially for those with chronic diseases. Biomolecular sensors, on the other hand, that measure the constituents of biological samples (e.g., blood, urine, saliva, etc.) provide a much more complete and medically relevant picture of the user's health. Such sensors could be used for at-home diagnosis of infection, monitoring of treatment progression [2]–[4], hydration and fatigue tracking during exercise [5], and testing food and water safety [2], [6]–[9].

While several add-on biosensing modules for mobile phones have been developed that leverage intrinsic hardware such as the camera, Bluetooth, USB, and audio port [2]–[18], these devices are still external to the phone making them more burdensome to manage and transport than a fully integrated solution, dissuading frequent use. By integrating biosensors directly into a smartphone or smartwatch (Fig. 1) and leveraging the scalability, cost-effectiveness, and accuracy of electrochemical biosensing, which led to the success of glucose meter,

Manuscript received February 8, 2016; revised April 24, 2016; accepted May 28, 2016. Date of publication September 26, 2016; date of current version December 7, 2016. This work was supported in part by Google's Advanced Technologies & Projects (ATAP). The views and opinions expressed in this article are those of the authors and do not necessarily reflect that of the funding agency. This paper was recommended by Associate Editor D. Demarchi.

The authors are with the Department of Electrical and Computer Engineering, University of California, San Diego, La Jolla, CA 92093 USA (e-mail: acs009@ucsd.edu; agvenkatesh@eng.ucsd.edu; drewhall@ucsd.edu).

Color versions of one or more of the figures in this paper are available online at http://ieeexplore.ieee.org.

Digital Object Identifier 10.1109/TBCAS.2016.2586504

one can develop much more accessible and seamless mHealth applications that promote adherence to frequent or continuous testing. Furthermore, in addition to being a boon for those who live with chronic illnesses, biosensors integrated into everyday items also enable other individuals who are either at risk for disease, trying to improve health and fitness, or curious about their well-being to routinely monitor themselves.

To this end, we describe the design of an electrochemical biosensor module for direct integration into a smartphone or wearable through the use of a reconfigurable bipotentiostat capable of both supporting an extended range of techniques and, at the same time, conforming to the challenging size and power consumption constraints set by continually shrinking portable devices. While enabling a wide variety of tests would typically consume additional area and power, this design alleviates the problem by repurposing the same components in different measurement modes, ultimately reducing the redundancy. The entire platform (Fig. 1) consists of the sensing module that houses the reconfigurable potentiostat that is meant to be built into a mobile device, an external sensor (disposable test strips, screen-printed electrodes, ion selective electrodes, etc.), and the mobile device itself. Since the external sensor component is in contact with the biological sample and is meant to be disposable, it is not permanently integrated into the smartphone like the rest of the module. However, when compared to non-integrated biosensors, which have this same external sensor constraint, smartphone integration ultimately eliminates having to carry around an extra hardware component thereby increasing accessibility. The mobile platform used in this work is Google's Project Ara modular smartphone, which allows the user to swap out different components and customize the phone's hardware. This platform is ideal for biosensor integration because of its open and high-speed interface as well as its modularity that enables the smartphone to have biosensing, amongst many other, capabilities.

## II. Electrochemical Sensing Background

As with other state-of-the-art POC electrochemical biosensors, the most crucial component is the potentiostat, or the analog front-end, that interfaces with and controls the electrodes in contact with the sample. A typical electrochemical cell consists of a working electrode (WE), where the biochemical reaction occurs, and a reference electrode (RE), usually working in tandem with a counter electrode (CE) to set the potential of the cell. While there are numerous types of techniques which the potentiostat can conduct, each with varying sets of parameters, requirements, and advantages, all these methods essentially measure different aspects of the same phenomenon: the movement and displacement of charge at the interface between an electrode and an electrolytic solution, also known as an electrochemical cell. Equivalent circuit models of this electrochemical cell can be used to better understand the sensing mechanisms of various electrochemical techniques, thereby guiding the design and implementation as well as setting the requirements of the circuits tailored for each distinct test type.

Randles equivalent circuit [19], shown in Fig. 2 for a three electrode system, is the most widely used electrical model

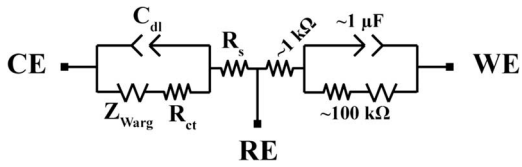


Fig. 2. Randles equivalent circuit model for a three electrode system.

for characterizing the electrode-solution interface, and contains four main components: double-layer capacitance ($C_{\rm dl}$), charge transfer resistance ($R_{\rm ct}$), Warburg impedance ($Z_{\rm Warg}$), and solution resistance ($R_s$). $C_{\rm dl}$ is a combination of the capacitance of the electrode itself and the capacitance generated by layers of ions and charged molecules forming at the surface of the electrode due to electrostatic forces. $C_{\rm dl}$ is not a strict capacitance, and is typically modelled as a constant phase element with an impedance of $Z_{\rm dl} = 1/((j\omega)^m C_{\rm dl})$, where $m$ is the phase parameter. $C_{\rm dl}$ ranges from 0.1–1 $\mu$F/mm$^2$ and is highly dependent on the salt concentration in solution as well as the voltage of the electrode [19], [20]. $R_{\rm ct}$ captures the transfer of electrons between the solution and electrode from reduction and oxidation reactions of molecules close to the surface. This resistance is $\sim$10–100 k$\Omega$ or approximately infinite in cases without the presence of redox molecules (non-faradic measurements) and varies with the concentration and type of molecule as well as the materials and voltage bias of the electrode. $Z_{\rm Warg}$ models the diffusion of redox molecules to and from the surface. Similar to $C_{\rm dl}$, it also is a constant phase element component, but always with a 45$^\circ$ phase shift. Finally, $R_s$ models the ions drifting in bulk solution and is set by the solution conductivity and applied voltage. Depending on the measurement technique, different components of this model become important to the design of the potentiostat.

Amperometry is the standard method to perform most sensitive labelled assays, which use enzymatic tags that transduce and amplify a detection event into a measurable electrochemical signal. The circuitry for amperometric techniques [21]–[22] applies a voltage waveform between the WE and RE using the CE to reduce voltage error while measuring the corresponding generated current signal at the WE, which is proportional to the concentration of the biomarker. For example, cyclic voltammetry (CV) and linear sweep voltammetry (LSV) both use slow (10–100 mV/s) ramps ($<$ 1 V sweep range) to stimulate the electrochemical cell, while step-techniques such as chronoamperometry (CA) and square wave voltammetry (SWV) instead use pulsed voltages (a single step for CA and 10–100 Hz for SWV). In the majority of amperometry, the objective is to measure the current due to a particular redox reaction rather than from the faster charging and discharging of $C_{\rm dl}$, referred to as background current. Even in pulsed techniques, the sections of the current measurement that contain the signal occur after the signal has settled. Hence, amperometry necessitates precise voltage control and high measurement sensitivity for slow, large signal currents.

While ions cannot be easily measured with traditional labelled assays or DC current measurements, their inherent charge and size allows them to be detected via potentiometric

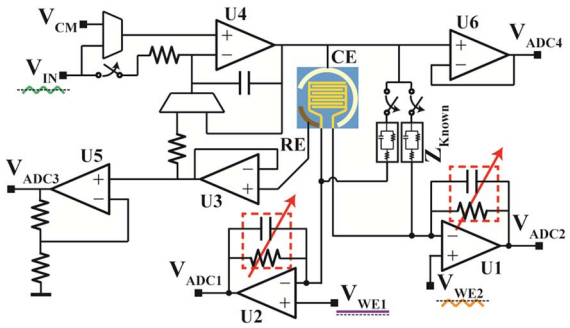


Fig. 3. Schematic of reconfigurable potentiostat where $V_{\mathrm{CM}}$, $V_{\mathrm{IN}}$, $V_{\mathrm{WE1}}$, and $V_{\mathrm{WE2}}$ are DAC outputs and $V_{\mathrm{ADC1-4}}$ are ADC inputs.

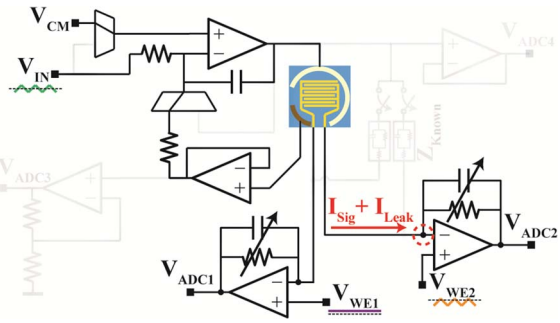


Fig. 4. Simplified schematic of the potentiostat in amperometric mode.

tests. Ion-selective electrodes (ISEs) separate specific ions with a semi-permeable membrane between two electrodes, thereby creating a potential difference (∼0.1–100 mV) proportional to the amount of that ion concentration in the solution. However, due to the nature of these sensors, their impedance is very high, roughly on the order of 100 MΩ, necessitating high resolution sampling of the electrode voltage with a high input impedance.

For label-free electrochemical assays, electrochemical impedance spectroscopy (EIS) is most often used since it measures changes in impedance on the surface of an electrode due to displacement of charge $(\Delta C_{\mathrm{dl}})$ or impeding of redox reactions $(\Delta R_{\mathrm{ct}})$. Although there are many different circuit topologies that can implement EIS [24]–[26], generally they all apply small amplitude (<10 mV) voltage sinusoids of varying frequencies (0.1 Hz–100 kHz) between a two electrode cell and record the resulting current. For each frequency, the magnitude and phase change is calculated and used to find the complex impedance ultimately forming an impedance spectrum that can be fitted to the Randles circuit. Unlike in traditional amperometry where aligning the timing of the input and output waveforms is often not necessary, EIS circuitry must not only have high enough bandwidth to measure these small signal AC currents but also have the ability to accurately track phase change between the applied voltage and measured current. Furthermore, any frequency dependent phase shift introduced by the measurement circuitry must be calibrated out.

## III. Design of Reconfigurable Module

In this work, the potentiostat discussed is based on a well-studied and commonly used topology in electrochemistry [27], [28], and is an expanded and improved version of our previous work [29]. However, to enable a large set of possible mHealth applications, the potentiostat must be able to run multiple types of techniques discussed above, which require different sensing modes and additional circuitry. Each of these various types of tests would typically require a different and separate set of circuitry. However, space and power are highly constrained resources on a mobile device and commodities must be shared with the device's other components. Therefore, in order to reduce the area and, more importantly when moving to an integrated circuit implementation, the power, a single reconfigurable design (Fig. 3), rather than three different sets of potentiostat circuits, is used that repurposes components from one mode to the next while maintaining performance across different techniques. Hence, the potentiostat is designed to support three distinct techniques: 1) amperometric, 2) potentiometric, and 3) impedance spectroscopy.

To further increase the flexibility and compatibility of the platform with POC type of tests, the potentiostat includes dual WEs each with its own resistive feedback transimpedance amplifier (TIA), which is based on circuit topology commonly used in potentiostats [30]–[32]. Using networks of switches that can switch between a range of different resistors and capacitors, each TIA has independently adjustable gain (10 kΩ, 100 kΩ, and 1 MΩ) and bandwidth (1 Hz–100 kHz), expanding its dynamic range and allowing it to measure different types of biomarkers that have varying sensitivity requirements. This dual WE functionality also enables two tests of the same technique to be run simultaneously on the same sample, allowing one to either be a control to compensate for factors such as temperature variation or background signals, or an additional sensor for another biomarker. In order to take advantage of this parallel testing, an assay must either generate no free-roaming redox molecules that can diffuse between electrodes and cause interference (e.g., label free assays) or use an electrode design that physically isolates or spreads out the sensing surfaces using wells or additional sample collection channels. Alternatively, the two electrodes can be used together for redox cycling with an interdigitated electrode in order to chemically amplify the signal for higher sensitivity, particularly when dealing with micro- and nano-scale sensors [33]. The common-mode voltage is adjustable to accommodate and optimize the various current and voltage ranges, which can be skewed either to the positive or negative side depending on the expected response. The different configurations and respective performance are discussed in the following sections.

### A. Amperometric

The potentiostat configuration for this mode is shown in Fig. 4. A voltage signal is applied to the three electrode sensor between the RE and the WE, with the CE supplying the current to set the solution potential. This voltage waveform, which varies depending on the technique chosen, generates a current signal in the solution that is measured at the WE, in this case, with a resistive feedback TIA. To expand the possible applications of the device, this potentiostat has two working electrodes with each channel having TIAs with independently

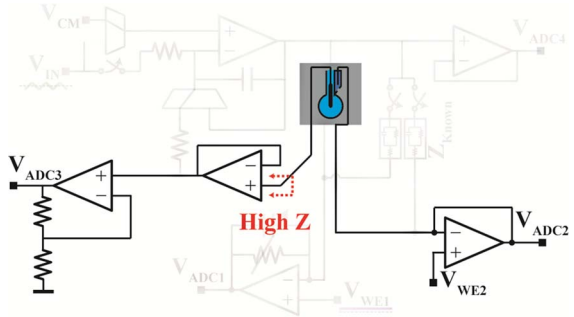


Fig. 5. Simplified schematic of the potentiostat in potentiometric mode.

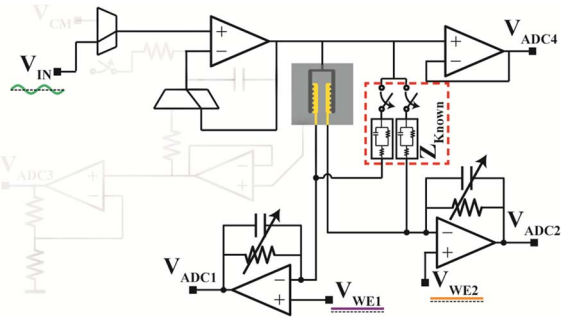


Fig. 6. Simplified schematic of the potentiostat in EIS mode.

configurable gain and bandwidth (adding either 1, 10, and 100 nF capacitor in parallel with the feedback resistance). The variable gain allows the device to adjust for the different baseline currents and varying physiological concentration ranges of different biomarkers, assays, and sensor areas. Also, since different amperometric techniques excite the electrochemical cell with different input voltage waveforms, the bandwidth of the generated current signal can vary.

Since the sensitivity of these measurements depends on how accurately current can be measured, the most important design considerations for this mode are the input-referred noise of the TIA and the current leakage at the WE node. Hence, all the switches where chosen to have low leakage ($<$ 20 pA) and the opamps (U1 and U2, Analog Devices AD8552) were selected to balance the power, input bias current (160 pA), and noise. The requirements at the other electrodes are less constrained. The input bias current of the RE circuitry must be minimized in order to reduce the IR error of the applied voltage. By using a very low input bias opamp (U3, Analog Devices AD8691) chosen specifically for the potentiometric mode (described later), this design achieves an RE leakage of 200 fA, which, with a typical solution resistance of 100 Ω, contributes a negligible 100 nV error. Furthermore, since the CE, which is controlled by U4 (Texas Instruments OPA2333), only needs to be able to supply the necessary current to the cell for this mode, the parameters for the control circuitry are set by the EIS mode.

### B. Potentiometric

In the potentiometric mode (Fig. 5), the voltage generated between two electrodes in a solution is measured. Typically, an ISE requires measurement circuitry with an input bias current of less than 1 pA to ensure that measurement error is less than 1%. Without adding a new set of components, the input buffer used for RE in the amperometric mode is switched into the signal path for use as a high impedance input with a working electrode operating as the other terminal. By adjusting the bandwidth switches to provide a short, the WE circuitry in this case operates as a buffer and allows the voltage from the sensor to either be sampled single-ended or pseudo-differentially to reject common-mode signals.

### C. Impedance Spectroscopy

In the EIS mode (Fig. 6), a two-electrode sensor is attached between the CE and a single WE, with the option of attaching an additional sensor on the other WE. Small signal (20 mV) voltage sinusoids, with varying frequency from 1 Hz–10 kHz, are applied between the two terminals and the WE measures the resulting current. The gain and bandwidth of the WE TIA is adjusted depending on the impedance and frequency being measured, changing if the signal is too small or if the channel becomes saturated. In the two other modes, the open switches and unused electrodes are always low impedance nodes set to known voltages in order to avoid instability and interference. However, in the EIS mode, the RE input is left floating in the circuitry in order to avoid the leakage current from adding a switch at this node, which is crucial for accurate amperometric and potentiometric measurements. However, the RE can be tied directly to the CE through a short on the electrode without affecting the impedance measurements as it can be incorporated into the calibration.

Making the approximation that the system is linear, due to the stimulus being small, the complex impedance $Z_{\mathrm{Cell}}$ is computed as

$$Z_{\mathrm{Cell}}(j\omega) = H(j\omega)\frac{V_{\mathrm{IN}}(j\omega)}{V_{\mathrm{OUT}}(j\omega)} \tag{1}$$

where $H(j\omega)$ is the transfer function that converts the current to voltage, $V_{\mathrm{IN}}$ is the voltage sinusoid applied to the $Z_{\mathrm{Cell}}$, and $V_{\mathrm{OUT}}$ is the voltage read by the ADC. $H(j\omega)$ is not only dependent on the feedback network of the TIA, which changes depending on the cell impedance, but also other factors such as parasitics in the switching networks and phase shift in the signal path. Hence, to account for varying $H(j\omega)$ and compensate the channel accordingly, known test impedances $(Z_{\mathrm{Known}})$ measured prior to use, one for each WE, are switched in between the two electrodes, given the same stimulus, and measured at each frequency before the actual sensor is tested

$$\begin{aligned} H(j\omega) &= Z_{\mathrm{Known}}(j\omega)\frac{V_{\mathrm{IN}}(j\omega)}{V_{\mathrm{Measured}}(j\omega)} \\ Z_{\mathrm{Known}}(j\omega) &= R_s + \frac{1}{j\omega C}||R_{\mathrm{ct}}. \end{aligned} \tag{2}$$

Using known impedance measurements, the transfer function of the channel can be determined for each frequency [Eq. (2)] and used to calibrate the impedance measurements in software on the host device [34]. Furthermore, to ensure that the input signal is correctly aligned with the output, the ADC simultaneously measures the CE voltage, thereby reducing phase error introduced by the control circuitry.

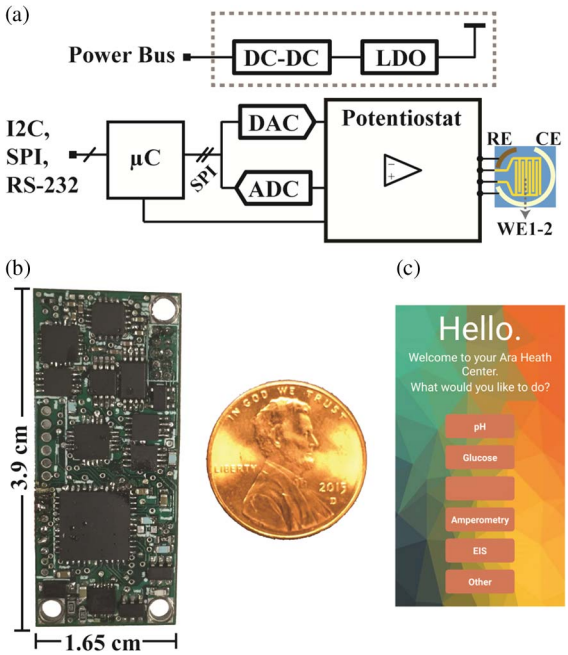


Fig. 7. (a) Block diagram of the entire module. (b) Photograph of PCB next to a US penny for scale. (c) Screenshot of smartphone application interface.

## IV. Integration With Mobile Technology

Shown in Fig. 7(a), aside from the potentiostat, the module also contains a power regulation network, a DAC (Analog Devices AD5685R), an ADC (Analog Devices AD7682), and a microcontroller (Microchip dsPIC33EP256MC204). This periphery circuitry can be easily tailored to the specifications of the wearable or mobile device. The design takes its power from the host device with an input voltage anywhere from 2.5 to 5.5 V and with a light-load efficient buck-boost DC-DC converter (Texas Instruments LM366SD) in series with two LDOs (Texas Instruments TPS79101) regulates it to both a 4 V and a 3.3 V thereby isolating the analog and digital supplies. The DAC (14-bits) and ADC (16-bits) both have 4 channels, and, via SPI, their maximum update and sample rates are ∼200 kHz. The microcontroller controls the potentiostat during testing by updating and sampling from the proper DAC and ADC channels respectively. The microcontroller also communicates with the host device via serial communication (either SPI, $I^2C$, or RS-232 depending on the mobile device interface) and configures the potentiostat with the proper settings. In order to integrate this module into a mobile device that is not a modular smartphone, an internal I/O port needs to be accessible. While this communication between the module and processor would usually be through a proprietary communication protocol, it is reasonable to expect that for mobile devices that use different types of sensors (such as accelerometers and pulse oximeters) the translation hardware is already available that implements the required communication interface between sensors and the high-speed processor bus. Hence, adding this module would be as simple as integrating any other sensor.

A $3.9 \times 1.65$ cm$^2$ 4-layer PCB [Fig. 7(b)] with discrete ICs was fabricated to fit into the Google Project Ara smartphone as a $2 \times 1$ sized module and work with an Android application [Fig. 7(c)]. Furthermore, this current prototype is small enough to be considered compatible with wearable devices as well. The module communicates with the Spiral 1 Ara platform via the $I^2C$ serial communication pins of the microcontroller. For testing purposes, we used several off-the-shelf sensors that each have varied connectors. Hence, an interposer board to accommodate all the electrodes was also constructed and attaches to the top or bottom of the module. Since the sensing areas are smaller than the module itself, actual developed and complete mobile devices can have the sensor or the sensor holder, in the case of disposable test strips, mounted directly into the shell of the device without altering the form factor.

## V. Electrical Measurement Data

Each of the three modes were characterized and tested to verify their functionality. For the amperometric mode, since the sensitivity of these measurements depends on how accurately current can be measured, the most important design considerations for this mode are the input-referred noise, which was measured with 100 kΩ gain and a 1 kHz bandwidth to be 216 $\text{pA}_{\text{RMS}}$, and the leakage current at the input of the TIAs or WE. Since low leakage switches for selecting the gain and bandwidth are used and the number of connections to the inverting node are minimized, the overall input leakage (∼180 pA) is dominated by the input bias current of the opamp. Hence, we can measure bidirectional currents ranging from ∼500 pA to 200 $\mu$A, which is ideal for most POC applications. For the potentiometric mode, the input bias current of the measurement circuitry is ∼200 fA, setting the approximate input impedance at 5 TΩ. The input referred voltage noise is 1.06 $\mu\text{V}_{\text{RMS}}$ (10 Hz bandwidth), and the voltage offset is ∼400 $\mu$V. For EIS, when testing a known impedance of 100 kΩ in parallel with 1 $\mu$F from 1 Hz–10 kHz, the module was measured to have a 5% magnitude and a 6° phase error as compared with a benchtop EIS tool. This configuration and calibration scheme described previously can measure an impedance range of 50 Ω–10 MΩ.

To demonstrate the reproducibility and stability of all modes, a series of repeated measurements ($N = 100$) on known inputs was performed using both the smartphone integrated platform and a benchtop potentiostat (CH Instruments 750E) also referred to in this paper as CHI. For the amperometric mode, a signal current of 10 $\mu$A was generated by applying a voltage signal across a model of an electrochemical cell made from circuit components resembling a simplified version of Randles equivalent circuit model ($R_{\text{ct}} = 200$ kΩ, $C_{\text{dl}} = 2$ $\mu$F, and $R_s = 1$ kΩ). For the potentiometric mode, an input voltage of 0.5 V was applied directly from the sourcemeter across two electrodes. Finally, for EIS, the same circuit model was measured by both instruments to find the value of the charge transfer resistance. The results, shown in Fig. 8, show the mean and standard deviation of the measurements normalized to the CHI data. While the variance in the data from the module is larger than that of the benchtop potentiostat (1.41 nA versus 88.6 pA, 93.7 $\mu$V versus 16.3 $\mu$V, and 0.630 Ω versus 0.186 Ω),

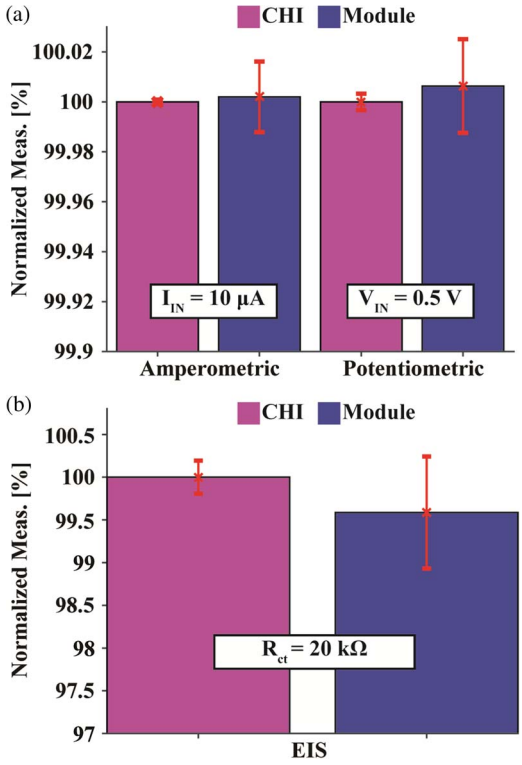


Fig. 8. (a) Plots of the amperometric, potentiometric, and (b) EIS mode repeated measurements for both the CHI and module potentiostat for $N = 100$ normalized to the CHI average.

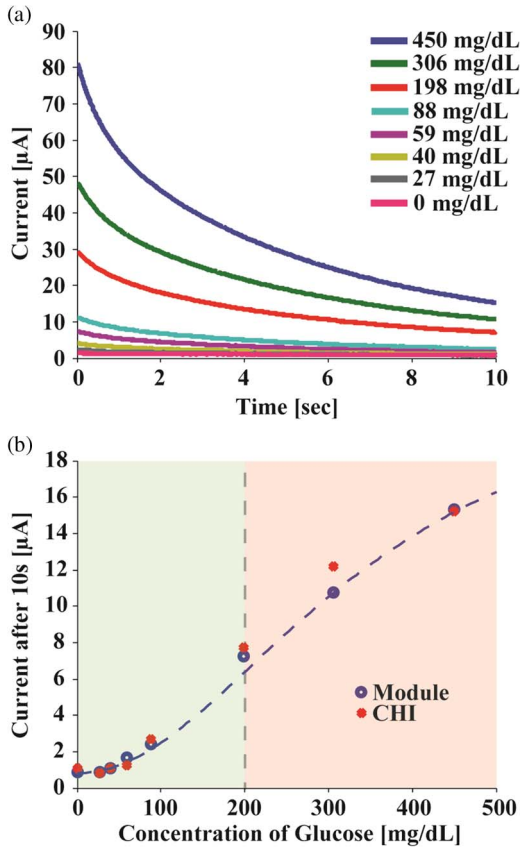


Fig. 9. (a) Chronoamperometry curves for glucose measured by the sensing module. (b) Calibration curves for both the biosensor and CHI with the positive and negative diagnosis ranges annotated.

each is still within acceptable bounds for that particular technique and matches well with the CHI measurements.

These modes also consume varying amounts of power, due to the different ADC sampling and data transfer rates required by each mode. Also, since the module can disable the potentiostat, ADC, and DAC, as well as make the microcontroller sleep, essentially shutting itself off when not measuring ($< 100\ \mu$W), the average runtimes of each technique also determine the overall energy used by each mode. The entire potentiostat's peak power consumption including the switches and multiplexors is 9.6 mW. To conserve space, many of the parts used in the potentiostat contain more than one device in a single package making it difficult to power gate individual unused components, so the power consumption of the potentiostat remains approximately constant across different modes. The digital and mixed signal circuitry including the microcontroller, ADC, and DAC consume a maximum of 49.5 mW in amperometric mode with a runtime of 10–200 s and 46.2 mW in potentiometric mode for tests that last approximately 10 s. In EIS mode, this power consumption is 111 mW for an average of 130 s. To put these numbers into context, the lithium ion battery found in most of today's smartphones has a capacity of approximately 1500 mAh. Average idle time is ∼50 hours (@ 108 mW), while talk time is ∼10 hours (@ 540 mW). Hence, at the very worst, this module would about match the power consumption of the phone while idling, and consume 80% less than a phone call. Therefore, making a couple of several minute-long measurements per day should not add noticeably to the battery drain of the mobile device.

## VI. Testing POC Applications

While the device itself can perform many types of electrochemical tests, the biomarkers detected in the following assays were chosen due to their POC applications. All these experiments, while some taking more effort and materials than others, do not require lab equipment to pre-process the samples and are possible to measure at the POC.

### A. Amperometric Testing

*1) Glucose:* For Glucose experiments, PBS was spiked with various concentrations of Dextrose from Marcon (4912-12) to create the test solutions. Commercial glucose test strips (True Test Blood Glucose Strips) based on Glucose dehydrogenase-PQQ (GDH) were applied with the various test solutions (27-450 mg/dL) and measured with chronoamperometry (0.5 V step for 10 seconds) with both a benchtop instrument (CHI 750E) and the biosensor module. Since commercial glucose strips are optimized for small droplets of blood (a few microliters), 1 $\mu$L of each of the test solutions were used in these measurements. The results (Fig. 9) show that the measured currents (taken after 10 seconds) for each concentration measured by both instruments follow the same trend. The calibration curve demonstrates that the assay is in the correct region to be able to diagnose or monitor diabetes (positive $>$ 200 mg/dL according to the American Diabetes Association).

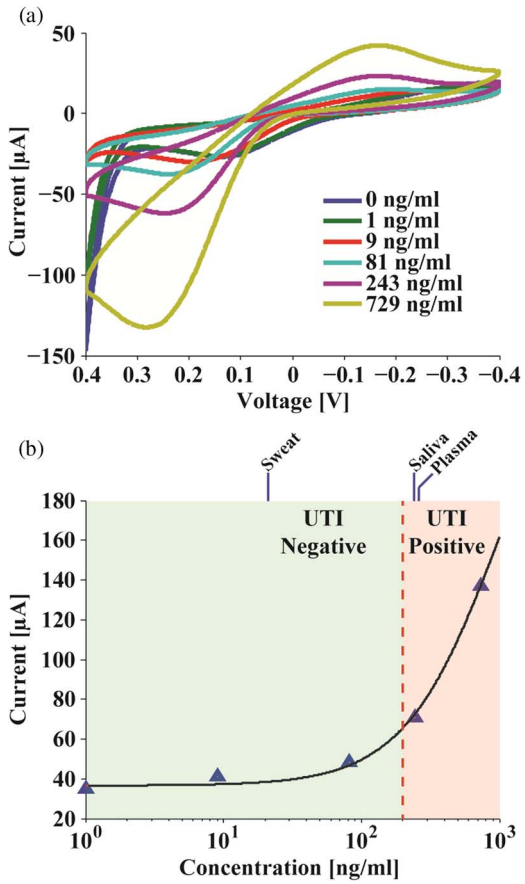


Fig. 10. (a) CV curves for LTF measured by the sensing module. (b) Calibration curves for the LTF assay with the positive and negative diagnosis ranges annotated.

*2) Lactoferrin:* Lactoferrin (LTF) is a common biomarker for infection found in various concentrations in bodily fluid such as sweat [35], saliva [36], urine [37], tears [38], and stool [39]. In this case, the detection of LTF in urine is used to diagnose urinary tract infection. Unlike the detection of glucose which is enzymatic, the detection method used here is a sandwich assay similar to an ELISA.

Gold DropSens electrodes were functionalized for detection of LTF. Anti-human LTF (Abcam #ab10110) was mixed with Traut's reagent (Pierce 26101), dropped on the gold working electrodes, and incubated overnight at $-4$ °C. 2% BSA (Thermo Scientific 37525) was applied for 1 hour at room temperature to block the surface. Afterwards, various concentrations of LTF (Abcam #a78526) in 20 $\mu$L droplets were added to each electrode before adding the secondary antibody (Abcam #ab25811) and then the NeutrAvidin conjugated alkaline phosphatase (Thermo Scientific #31002). Each binding step lasted an hour and included washing in between. Finally, before running cyclic voltammetry on each electrode, the substrate, p-AminoPhenyl Phosphate (Santa Cruz Biotechnology sc-281392) was added and allowed to react for 10 minutes. The sweep range and scan rate were $-0.2$ V to 0.3 V and 25 mV/s, respectively.

The concentration of LTF in the urine of a patient with and without an UTI is $3300 \pm 646.3$ ng/mL and $60.3 \pm 14.9$ ng/mL, respectively [37]. As shown in Fig. 10, the limit of detection

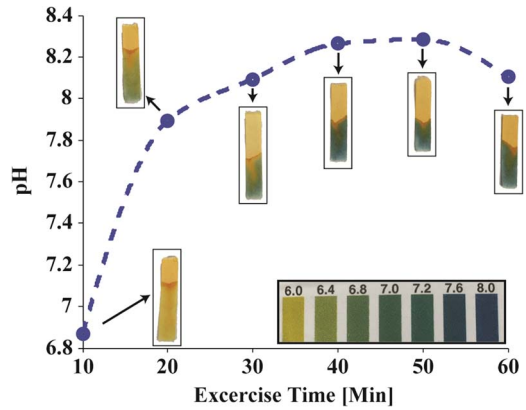


Fig. 11. Plot of pH levels of sweat from subject during exercise and the pH test strip result for each sample.

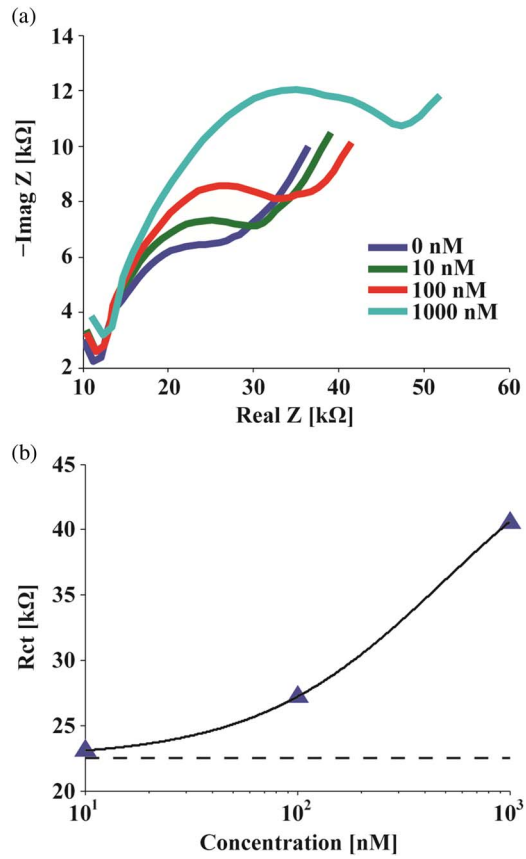


Fig. 12. (a) Nyquist plot of each serial dilution of NeutraAvidin. (b) Concentration curve after fitting data to the Randles circuit to find charge transfer resistance with baseline drawn below.

of this assay is approximately $\sim$1 ng/mL. Hence, LTF can be detected by this device in the diagnostically relevant range. Furthermore, the average LTF concentration in various bodily fluids in healthy patients is annotated on the same plot, demonstrating that this device could also be used to measure physiological LTF concentrations in these other fluids.

### *B. pH Measurements in Sweat*

pH levels in sweat secreted from the skin have been shown to correlate with hydration levels in the body [5]. The higher

TABLE I
COMPARISON WITH STATE OF THE ART FOR ALL ELECTROCHEMICAL MODES

| Ref. | Amperometric | | Potentiometric | | EIS | | |
|---|---|---|---|---|---|---|---|
| | Dynamic Range | Sensitivity [nA] | pH Resolution | Input Z [Ω] | Frequency [Hz] | Z Range [Ω] | Mag. / Phase Error |
| [29] | 54 dB (50 μA max) | 100 | - | - | - | - | - |
| [39] | 43.5 dB (750 μA max) | 5000 | - | - | - | - | - |
| [40] | 51.1 dB (5.4 μA max) | 15 | - | - | - | - | - |
| [2] | 104 dB (78 μA max) | 0.5 | 8% | 5 TΩ | - | - | - |
| [5] | - | - | 0.2 pH | N/A | - | - | - |
| [41] | - | - | - | - | 0.01 – 100k | 1k-1T | 5%, 3° |
| [42] | - | - | - | - | 10 – 100k | N/A | 12.3%, 12° |
| [15] | - | - | - | - | 10 – 10k | 1k – 10M | N/A, 0.8° |
| ***This Work*** | ***106 dB (200 μA max)*** | ***< 1 nA*** | ***1.2%, 0.08 pH*** | ***~5 TΩ*** | ***1 – 10k*** | ***50 – 10M*** | ***5%, 6°*** |

the pH the more dehydrated someone is. Hence, by monitoring sweat during exercise, hydration can be tracked allowing the user to act accordingly to optimize his or her workout and avoid dangerous over exertion.

In order to first test the potentiostatic mode's accuracy when interfaced with a high impedance sensor, standard pH buffers from Thermo Scientific (910104, 910107, and 910110) were used as well as separately prepared phosphate buffers adjusted to specific values ranging from pH 4–10. All measurements were taken with an Oakton pH Probe (EW-35811-74). These buffers were measured with the biosensor module in potentiometric mode and verified with a table top pH meter (Orion Star A211). The maximum deviation was found to be 1.2% or 0.08 pH between the two measurement methods.

Next, 75 $\mu$L of sweat was collected at 10-minute intervals from a volunteer running at a steady pace for an hour. Afterwards, the sweat was tested with the module using a small pH electrode (VersaFlex VNIS/LD). Each sample was also tested using standard pH test strips (pHydrion Vivid 67). As shown in Fig. 11, the pH level increases steadily as more sweat is lost during the exercise as expected when compared to published data [5]. The test strips line up with the pH levels measured by the device and serve to confirm this trend as well.

### C. Label-Free Assay

The sensing of certain biomarkers, such as ions (H+, Na+, etc.) and some metabolites (glucose, lactose, etc.) especially those with large physiological concentrations, can be easily designed for portable POC use without an abundance of steps or reagents. However, assays for more complex molecules (peptides, proteins, DNA, etc.) that require much higher sensitivity to detect can be more cumbersome and time consuming for a user to conduct. For infrequent diagnostic tests, such as the labelled and highly sensitive UTI test discussed previously, the additional washing and reagent steps in the assay are manageable in the case of at-home testing. However, for more remote applications that require equally high sensitivity and increased portability, label-free techniques, such as EIS, are a promising solution as they do not use enzymatic labels to indirectly measure the biomarker, but rather physical and chemical changes, allowing for faster results with fewer assay steps [44], [45]. To demonstrate our module's label-free capabilities, we conducted an assay for the detection of NeutrAvidin using biotin immobilized on the surface of a gold electrode. NeutrAvidin is version of avidin, a protein that forms a specific and high-affinity bond with biotin, a pair commonly used as a preliminary model for label-free detection assays.

Prior to the start of the assay, the electrode, 100 nm of gold sputtered onto a glass substrate, was cleaned with 1 mM $KOH/H_2O_2$ and functionalized with a 100 $\mu$M thiolated-biotin (Sigma-Aldrich #746622) reagent solution. After performing a washing and blocking, the electrode was ready for use. 20 $\mu$L droplets of different concentrations of NeutrAvidin (Thermo Scientific #31000) in a 1 mM ferro/ferri-cyanide ($K_4[Fe(CN)_6]$)/$K_3[Fe(CN)_6]$) PBS buffer were added to the electrode, allowed to bind for 10 minutes, and then measured using EIS (1 Hz–10 kHz) with a Ag wire pseudo RE. These data were then fitted against the standard Randles circuit [19] to determine the change in charge transfer resistance, relevant in faradaic impedance measurements. The Nyquist plot of the results as well as the concentration curve, shown in Fig. 12, clearly demonstrate that this module can be used as a label-free biosensor. While NeutrAvidin itself is not a particularly useful biomarker, due to the mechanism of the biotin-avidin bonding, the results of this model assay demonstrate that this device can be generalized and used in most label-free affinity assays already developed [46]–[48].

### D. Comparison With Literature

These POC applications experiments demonstrate both the performance and the extensive functionality of the reconfigurable module. To closely examine the performance, Table I shows a comparison with state-of-the-art portable biosensors that have been previously published. For each mode, our module approximately matches the performance of other platforms in terms of dynamic range, sensitivity, and error, while at the same time being able to reconfigure itself into these three different sensing modes. Hence, whereas other devices only have one or two of these measurement capabilities, this device is able to package all these multiple techniques with approximately equivalent performance into a single small form factor module.

## VII. CONCLUSION

We have built and demonstrated a reconfigurable, multi-technique biosensor platform specially designed for integration directly into mobile devices for diagnosing and monitoring the health of a user at the POC. By reusing components in different measurement modes, we can minimize the size and power of the design while at the same time keeping performance and

expanding the functionality of the module for use in most POC applications. By adding this dedicated hardware directly into every day carry electronics, we hope to promote the use of specialized, portable, and practical medical devices well positioned to be the first line of defense in the future of healthcare.

## ACKNOWLEDGMENT

The authors acknowledge T. Phelps for his help programming the Android smartphone application.

## REFERENCES

[1] B. W. Ward, J. S. Schiller, and R. A. Goodman, "Multiple chronic conditions among US adults: A 2012 update," *Prev. Chronic. Dis.*, vol. 11, Apr. 2014.

[2] A. Nemiroski, D. C. Christodouleas, J. W. Hennek, A. A. Kumar, E. J. Maxwell, M. T. Fernández-Abedul, and G. M. Whitesides, "Universal mobile electrochemical detector designed for use in resource-limited applications," *Proc. Nat. Acad. Sci.*, vol. 111, no. 33, pp. 11984–11989, Aug. 2014.

[3] P. B. Lillehoj, M.-C. Huang, N. Truong, and C.-M. Ho, "Rapid electrochemical detection on a mobile phone," *Lab. Chip*, vol. 13, no. 15, pp. 2950–2955, Jul. 2013.

[4] B. Berg, B. Cortazar, D. Tseng, H. Ozkan, S. Feng, Q. Wei, R. Y.-L. Chan, J. Burbano, Q. Farooqui, M. Lewinski, D. Di Carlo, O. B. Garner, and A. Ozcan, "Cellphone-based hand-held microplate reader for point-of-care testing of enzyme-linked immunosorbent assays," *ACS Nano*, vol. 9, no. 8, pp. 7857–7866, Aug. 2015.

[5] V. Oncescu, D. O'Dell, and D. Erickson, "Smartphone based health accessory for colorimetric detection of biomarkers in sweat and saliva," *Lab. Chip*, vol. 13, no. 16, pp. 3232–3238, Jul. 2013.

[6] X. Wang, M. R. Gartia, J. Jiang, T.-W. Chang, J. Qian, Y. Liu, X. Liu, and G. L. Liu, "Audio jack based miniaturized mobile phone electrochemical sensing platform," *Sens. Actuators B, Chem.*, vol. 209, pp. 677–685, Mar. 2015.

[7] C. Ionescu, P. Svasta, C. Tamas, C. Bala, and L. Rotariu, "Portable measuring and display unit for electrochemical sensors," in *Proc. IEEE 16th Int. Symp. Design Technol. Electron. Packaging*, 2010, pp. 215–218.

[8] S. K. J. Ludwig, C. Tokarski, S. N. Lang, L. A. van Ginkel, H. Zhu, A. Ozcan, and M. W. F. Nielen, "Calling biomarkers in milk using a protein microarray on your smartphone," *PLoS ONE*, vol. 10, no. 8, Aug. 2015, Art. no. e0134360.

[9] S. K. J. Ludwig, H. Zhu, S. Phillips, A. Shiledar, S. Feng, D. Tseng, L. A. van Ginkel, M. W. F. Nielen, and A. Ozcan, "Cellphone-based detection platform for rbST biomarker analysis in milk extracts using a microsphere fluorescence immunoassay," *Anal. Bioanal. Chem.*, vol. 406, no. 27, pp. 6857–6866, Jun. 2014.

[10] C. M. McGeough and S. O'Driscoll, "Camera phone-based quantitative analysis of c-reactive protein ELISA," *IEEE Trans. Biomed. Circuits Syst.*, vol. 7, no. 5, pp. 655–659, Oct. 2013.

[11] L. Cevenini, M. M. Calabretta, G. Tarantino, E. Michelini, and A. Roda, "Smartphone-interfaced 3D printed toxicity biosensor integrating bioluminescent 'sentinel cells," *Sens. Actuators B, Chem.*, vol. 225, pp. 249–257, Mar. 2016.

[12] K. Su, Q. Zou, J. Zhou, L. Zou, H. Li, T. Wang, N. Hu, and P. Wang, "High-sensitive and high-efficient biochemical analysis method using a bionic electronic eye in combination with a smartphone-based colorimetric reader system," *Sens. Actuators B, Chem.*, vol. 216, pp. 134–140, Sep. 2015.

[13] W. Xu, S. Lu, Y. Chen, T. Zhao, Y. Jiang, Y. Wang, and X. Chen, "Simultaneous color sensing of O2 and pH using a smartphone," *Sens. Actuators B, Chem.*, vol. 220, pp. 326–330, Dec. 2015.

[14] M. Zangheri, L. Cevenini, L. Anfossi, C. Baggiani, P. Simoni, F. Di Nardo, and A. Roda, "A simple and compact smartphone accessory for quantitative chemiluminescence-based lateral flow immunoassay for salivary cortisol detection," *Biosens. Bioelectron.*, vol. 64, pp. 63–68, Feb. 2015.

[15] D. Zhang, Y. Lu, Q. Zhang, L. Liu, S. Li, Y. Yao, J. Jiang, G. L. Liu, and Q. Liu, "Protein detecting with smartphone-controlled electrochemical impedance spectroscopy for point-of-care applications," *Sens. Actuators B, Chem.*, vol. 222, pp. 994–1002, Jan. 2016.

[16] E. H. Doeven, G. J. Barbante, A. J. Harsant, P. S. Donnelly, T. U. Connell, C. F. Hogan, and P. S. Francis, "Mobile phone-based electrochemiluminescence sensing exploiting the 'USB On-The-Go' protocol," *Sens. Actuators B, Chem.*, vol. 216, pp. 608–613, Sep. 2015.

[17] A. Sun, T. Wambach, A. G. Venkatesh, and D. A. Hall, "A low-cost smartphone-based electrochemical biosensor for point-of-care diagnostics," in *Proc. IEEE Biomedical Circuits Systems Conf.*, 2014, pp. 312–315.

[18] A. C. Sun, C. Yao, V. A. G., and D. A. Hall, "An efficient power harvesting mobile phone-based electrochemical biosensor for point-of-care health monitoring," *Sensors and Actuators B: Chemical*, vol. 235, pp. 126–135, Nov. 2016.

[19] A. J. Bard and L. R. Faulkner, *Electrochemical Methods Fundamentals and Applications*, 2nd ed. Hoboken, NJ, USA:Wiley, 2001.

[20] H.-J. Butt, K. Graf, and M. Kappl, *Physics and Chemistry of Interfaces*, 2nd ed. Weinheim, Germany: Wiley-VCH, 2006.

[21] M. H. Nazari, H. Mazhab-Jafari, L. Leng, A. Guenther, and R. Genov, "CMOS neurotransmitter microarray: 96-channel integrated potentiostat with on-die microsensors," *IEEE Trans. Biomed. Circuits Syst.*, vol. 7, no. 3, pp. 338–348, Jun. 2013.

[22] M. M. Ahmadi and G. A. Jullien, "Current-mirror-based potentiostats for three-electrode amperometric electrochemical sensors," *IEEE Trans. Circuits Syst. I, Reg. Papers*, vol. 56, no. 7, pp. 1339–1348, Jul. 2009.

[23] M. Stanacevic, K. Murari, A. Rege, G. Cauwenberghs, and N. V. Thakor, "VLSI potentiostat array with oversampling gain modulation for wide-range neurotransmitter sensing," *IEEE Trans. Biomed. Circuits Syst.*, vol. 1, no. 1, pp. 63–72, Mar. 2007.

[24] A. Manickam, A. Chevalier, M. McDermott, A. D. Ellington, and A. Hassibi, "A CMOS Electrochemical Impedance Spectroscopy (EIS) Biosensor Array," *IEEE Trans. Biomed. Circuits Syst.*, vol. 4, no. 6, pp. 379–390, Dec. 2010.

[25] A. Carullo, F. Ferraris, M. Parvis, A. Vallan, E. Angelini, and P. Spinelli, "Low-cost electrochemical impedance spectroscopy system for corrosion monitoring of metallic antiquities and works of art," *IEEE Trans. Instrum. Meas.*, vol. 49, no. 2, pp. 371–375, Apr. 2000.

[26] H. Jafari, L. Soleymani, and R. Genov, "16-Channel CMOS impedance spectroscopy DNA analyzer with dual-slope multiplying ADCs," *IEEE Trans. Biomed. Circuits Syst.*, vol. 6, no. 5, pp. 468–478, Oct. 2012.

[27] M. Vergani, M. Carminati, G. Ferrari, E. Landini, C. Caviglia, A. Heiskanen, C. Comminges, K. Zor, D. Sabourin, M. Dufva, M. Dimaki, R. Raiteri, U. Wollenberger, J. Emneus, and M. Sampietro, "Multichannel bipotentiostat integrated with a microfluidic platform for electrochemical real-time monitoring of cell cultures," *IEEE Trans. Biomed. Circuits Syst.*, vol. 6, no. 5, pp. 498–507, Oct. 2012.

[28] L. Li, X. Liu, W. A. Qureshi, and A. J. Mason, "CMOS amperometric instrumentation and packaging for biosensor array applications," *IEEE Trans. Biomed. Circuits Syst.*, vol. 5, no. 5, pp. 439–448, Oct. 2011.

[29] A. Sun, T. Wambach, A. G. Venkatesh, and D. A. Hall, "A multitechnique reconfigurable electrochemical biosensor for integration into mobile technologies," in *Proc. IEEE Biomedical Circuits Syst. Conf.*, 2015, pp. 1–4.

[30] A. A. Rowe, A. J. Bonham, R. J. White, M. P. Zimmer, R. J. Yadgar, T. M. Hobza, J. W. Honea, I. Ben-Yaacov, and K. W. Plaxco, "CheapStat: An open-source, 'Do-It-Yourself' potentiostat for analytical and educational applications," *PLoS ONE*, vol. 6, no. 9, Sep. 2011, Art. no. e23783.

[31] S. Hwang and S. Sonkusale, "CMOS VLSI potentiostat for portable environmental sensing applications," *IEEE Sens. J.*, vol. 10, no. 4, pp. 820–821, 2010.

[32] I. Ramfos, N. Vassiliadis, S. Blionas, K. Efstathiou, A. Fragoso, C. K. O'Sullivan, and A. Birbas, "A compact hybrid-multiplexed potentiostat for real-time electrochemical biosensing applications," *Biosens. Bioelectron.*, vol. 47, pp. 482–489, Sep. 2013.

[33] J. Das, K. Jo, J. W. Lee, and H. Yang, "Electrochemical immunosensor using p-aminophenol redox cycling by hydrazine combined with a low background current," *Anal. Chem.*, vol. 79, no. 7, pp. 2790–2796, Apr. 2007.

[34] J. S. Daniels, E. P. Anderson, T. H. Lee, and N. Pourmand, "Simultaneous measurement of nonlinearity and electrochemical impedance for protein sensing using two-tone excitation," in *Proc. 30th Annu. Int. Conf. IEEE Engineering Medicine Biology Soc.*, 2008, pp. 5753–5756.

[35] J.-H. Park, G.-T. Park, I. H. Cho, S.-M. Sim, J.-M. Yang, and D.-Y. Lee, "An antimicrobial protein, lactoferrin exists in the sweat: proteomic analysis of sweat," *Exp. Dermatol.*, vol. 20, no. 4, pp. 369–371, 2011.

[36] F. Mizuhashi, K. Koide, S. Toya, M. Takahashi, R. Mizuhashi, and H. Shimomura, "Levels of the antimicrobial proteins lactoferrin and chromogranin in the saliva of individuals with oral dryness," *J. Prosthet. Dent.*, vol. 113, no. 1, pp. 35–38, 2015.

[37] S. Arao, S. Matsuura, M. Nonomura, K. Miki, K. Kabasawa, and H. Nakanishi, "Measurement of urinary lactoferrin as a marker of urinary tract infection," *J. Clin. Microbiol.*, vol. 37, no. 3, pp. 553–557, Mar. 1999.
[38] A. Kijlstra, S. H. Jeurissen, and K. M. Koning, "Lactoferrin levels in normal human tears.," *Br. J. Ophthalmol.*, vol. 67, no. 3, pp. 199–202, Mar. 1983.
[39] M. Joishy, I. Davies, M. Ahmed, J. Wassel, K. Davies, A. Sayers, and H. Jenkins, "Fecal Calprotectin and Lactoferrin as noninvasive markers of pediatric inflammatory bowel disease," *J. Pediatr. Gastroenterol. Nutr.*, vol. 48, no. 1, pp. 48–54, Jan. 2009.
[40] A. F. D. Cruz, N. Norena, A. Kaushik, and S. Bhansali, "A low-cost miniaturized potentiostat for point-of-care diagnosis," *Biosens. Bioelectron.*, vol. 62, pp. 249–254, Dec. 2014.
[41] M. D. Steinberg, P. Kassal, I. Kereković, and I. M. Steinberg, "A wireless potentiostat for mobile chemical sensing and biosensing," *Talanta*, vol. 143, pp. 178–183, Oct. 2015.
[42] E. Angelini, S. Corbellini, M. Parvis, F. Ferraris, and S. Grassini, "An Arduino-based EIS with a logarithmic amplifier for corrosion monitoring," in *Proc. IEEE Int. Instrum. Meas. Technol. Conf.*, 2014, pp. 905–910.
[43] J. Punter-Villagrasa, B. del Moral-Zamora, J. Colomer-Farrarons, P. Miribel-Catala, J. Cid, I. Rodriguez-Villarreal, and B. Prieto-Simon, "A portable point-of-use EIS device for in-vivo biomédical applications," in *Proc. Conf. Design Circuits Integr. Circuits*, 2014, pp. 1–6.
[44] J. S. Daniels and N. Pourmand, "Label-Free Impedance Biosensors: Opportunities and Challenges," *Electroanalysis*, vol. 19, no. 12, pp. 1239–1257, 2007.
[45] E. Katz and I. Willner, "Probing biomolecular interactions at conductive and semiconductive surfaces by impedance spectroscopy: Routes to impedimetric immunosensors, DNA-sensors, and enzyme biosensors," *Electroanalysis*, vol. 15, no. 11, pp. 913–947, 2003.
[46] M. Xu, X. Luo, and J. J. Davis, "The label free picomolar detection of insulin in blood serum," *Biosens. Bioelectron.*, vol. 39, no. 1, pp. 21–25, Jan. 2013.
[47] R. Ohno, H. Ohnuki, H. Wang, T. Yokoyama, H. Endo, D. Tsuya, and M. Izumi, "Electrochemical impedance spectroscopy biosensor with interdigitated electrode for detection of human immunoglobulin A," *Biosens. Bioelectron.*, vol. 40, no. 1, pp. 422–426, Feb. 2013.
[48] T. Bryan, X. Luo, P. R. Bueno, and J. J. Davis, "An optimised electrochemical biosensor for the label-free detection of C-reactive protein in blood," *Biosens. Bioelectron.*, vol. 39, no. 1, pp. 94–98, Jan. 2013.

**Alexander Sun** (S'13) received the B.S. degree in electrical engineering and computer science from the University of California, Berkeley, Berkeley, CA, USA, and the M.S. degree in electrical and computer engineering from the University of California, San Diego (UCSD), La Jolla, CA, USA, in 2012 and 2014, respectively.

Currently, he is working toward the Ph.D. degree at UCSD. His research focuses on electrochemical biosensors, electrochemical measurement techniques, and compact, low power circuit design for biomedical, and point-of-care devices.

**A. G. Venkatesh** received the B.Sc. degree in biochemistry from the University of Madras, Tamil Nadu, India, the M.Sc. degree in biotechnology from Bharathidasan University, Tamil Nadu, India, the M.Tech. degree in bioelectronics from Tezpur University, Assam, India, and the Ph.D. degree in physics from Bielefeld University, Bielefeld, Germany.

During his doctoral research, he developed a novel platform to monitor DNA-protein interactions in real-time and, as a Postdoctoral Researcher at the University of Freiburg, Freiburg im Breisgau, Germany, he developed low-cost, smartphone-based devices for biomedical applications. Currently, he is involved in developing smartphone-based electrochemical assays for clinical applications in the point-of-care domain at the University of California, San Diego, La Jolla, CA, USA. As an Interdisciplinary Researcher, he is interested in research that involves the integration of physics, chemistry, and biology.

**Drew A. Hall** (S'07–M'12) received the B.S. degree (honors) in computer engineering from the University of Nevada, Las Vegas, Las Vegas, NV, USA, in 2005, and the M.S. and Ph.D. degrees in electrical engineering from Stanford University, Stanford, CA, USA, in 2008 and 2012, respectively.

From 2011 to 2013, he was a Research Scientist at the Intel Corporation in the Integrated Biosensors Laboratory. Since 2013, he has been with the University of California, San Diego, La Jolla, CA, USA, as an Assistant Professor in the Department of Electrical and Computer Engineering. His research interests include bioelectronics, biosensors, analog circuit design, medical electronics, and sensor interfaces.

Dr. Hall was the corecipient of First Place in the inaugural International IEEE Change the World Competition and First Place in the BME-IDEA invention competition, both in 2009. He received the Analog Devices Outstanding Designer Award in 2011, an undergraduate teaching award in 2014, the Hellman Fellowship Award in 2014, and an NSF CAREER Award in 2015. He is a Tau Beta Pi Fellow.